MESHLESS APPROACHES FOR THE NUMERICAL RESOLUTION OF SINGULARLY PERTURBED BOUNDARY VALUE PROBLEMS WITH LAYERED SOLUTION STRUCTURES

J. CHRIST JENNIFER[1*] and Dr. S. SENDHAMIZH SELVI[2]

[1] Research Scholar, PG & Research Department of Mathematics, Government Arts College (Affiliated to Bharathidasan University), Trichy - 620 022, Tamil Nadu, India.
Email: jameschristjennifer@gmail.com

[2] Associate Professor, PG & Research Department of Mathematics, Government Arts College (Affiliated to Bharathidasan University), Trichy - 620 022, Tamil Nadu, India.
Email: sentamilselvis12@gmail.com

*** J. CHRIST JENNIFER – Corresponding Author**
Research Scholar, PG & Research Department of Mathematics, Government Arts College (Affiliated to Bharathidasan University), Trichy - 620 022, Tamil Nadu, India.
Email: jameschristjennifer@gmail.com

DOI: https://doi.org/10.63001/tbs.2026.v21.i04.S.I(4).pp928-941

KEYWORDS

Singularly perturbed boundary value problems, Meshless Collocation methods, layered solution structures, Point interpolation.

Article Info

Received: 09/08 /2026

Accepted: 29 /10/2026

Published: 05/11/2026

Abstract

To overcome the limitations of traditional mesh-based methods that struggle to capture steep gradients in Singularly Perturbed Boundary Value Problems (SPBVPs) with sharp boundary and interior layer structures without costly and complex mesh refinement. We investigate point interpolation and boundary-type meshless techniques that bypass mesh generation and flexibly adapt to complex layer phenomena by systematically decomposing solutions into regular and singular components, validated by numerical experiments with error and convergence analysis and reproducible Python implementations. The framework ensures computational stability, strong layer-resolving capabilities, and parameter-uniform convergence across all perturbation regimes, with numerical experiments validating the accuracy, efficiency, and robustness of the methods. Presents Meshless point interpolation and boundary-type techniques with solution decomposition to resolve complex layer phenomena in SPBVPs without mesh generation.

1.Introduction

Singularly perturbed boundary value problems (SPBVPs) model convection-diffusion phenomena characterized by sharp boundary or interior layers, where standard numerical schemes experience severe stability losses as the perturbation parameter approaches zero. Although recent advancements such as meshless Radial Basis Function techniques [1], domain decomposition frameworks [2], dual-layer exponential fitting methods [3], and higher-order compact finite-difference schemes [4] have addressed these multiscale difficulties, existing methodologies face significant drawbacks. Specifically, meshless techniques frequently suffer from severe matrix ill-conditioning and sensitivity to shape parameters, whereas layer-adapted and fitted schemes incur high computational costs and algorithmic complexity when extended to complex systems. To directly rectify these limitations, this study presents a robust, parameter-

uniform, and computationally efficient numerical framework that accurately resolves steep transition layers without sacrificing matrix condition numbers or requiring complex grid adjustments. The objectives of this study are to develop a meshless point interpolation scheme that resolves boundary and interior layers without mesh generation, to establish parameter-uniform stability and convergence theoretically, and to validate accuracy and robustness through numerical experiments across perturbation regimes.

2. Material and Method:

2.1 Problem Formulation and Layer Analysis

We consider singularly perturbed differential equations of the form

$$Lu(x)=-\varepsilon u''(x)+a(x)u'(x)+b(x)u(x)=f(x), x \in \Omega=[x_L,x_R]$$

subject to Dirichlet boundary $u(x_L)=\alpha, u(x_R)=\beta$ where $\varepsilon \in (0,1]$ is the small perturbation parameter, $a(x), b(x), f(x)$ are sufficiently smooth functions on $\Omega, b(x) \geq b_0>0$ ensures the problem is well-posed and $a(x)$ may vanish at interior points (turning points). This equation often arises as the steady-state limit of time-dependent problems of the form, $\frac{\partial u}{\partial t}=\varepsilon\frac{\partial^2 u}{\partial x^2}-a(x)\frac{\partial u}{\partial x}-b(x)u+f(x)$. The singular nature of the problem leads to solutions with distinct behavioral regions: **1. Outer region:** Described by the reduced solution $u_0(x)$ obtained by setting $\epsilon=0$, giving $a(x)u_0'(x)+b(x)u_0(x)=f(x)$, **2. Boundary layers:** Narrow regions of width $O(\epsilon)$ where the solution transitions exponentially to satisfy boundary conditions, **3. Interior layers:** Regions of width $O(\sqrt{\epsilon})$ formed near an interior turning point x_0 where $a(x_0)=0$.

2.1.1 Minimum Principle and Stability Estimate:

Lemma 2.1 (Minimum Principle). Let $u(x) \in C^2(\Omega)$ satisfy $Lu(x)=-\varepsilon u''(x)+a(x)u'(x)+b(x)u(x) \geq 0, \forall x \in \Omega$ with boundary conditions $u(x_L) \geq 0, u(x_R) \geq 0$ and $b(x) \geq b_0>0$. Then $u(x) \geq 0$ for all $x \in \Omega$.

Theorem 2.1 (Stability Estimate). The solution $u(x)$ of the singularly perturbed boundary value problem satisfies: $\|u\|_\infty \leq C(\|f\|_\infty+|\alpha|+|\beta|)$ where $C>0$ is a constant independent of ε, and $\|\cdot\|_\infty$ denotes the maximum norm on Ω.

2.1.2 Derivative Bounds and Asymptotic Layer Structure:

Lemma 2.2 (Derivative Bounds)

Let the solution $u(x)$ be decomposed as $u(x)=v(x)+w_L(x)+w_R(x)$ where $v(x)$ is the smooth (regular) component and $w_L(x), w_R(x)$ are boundary layer components. Then for all $x \in \Omega$ and $\kappa=0,1,2$: $\left|v^{(\kappa)}(x)\right| \leq C$, $\left|w_L^{(\kappa)}(x)\right| \leq C\varepsilon^{-\kappa} exp\left(-\frac{\lambda(x-x_L)}{\varepsilon}\right)$ and $\left|w_R^{(\kappa)}(x)\right| \leq C\varepsilon^{-\kappa} exp\left(-\frac{\lambda(x_R-x)}{\varepsilon}\right)$ for constants $C, \lambda>0$ independent of ε.

Proof. The solution is given explicitly by $v(x)=e^{-\int \frac{b(s)}{a(s)}ds}\left[\alpha+\int e^{\int \frac{b(s)}{a(s)}ds}\frac{f(t)}{a(t)}dt\right]$..

Since $a, b, f \in C^2(\Omega)$ with $a(x) \neq 0$, the regular solution satisfies $v \in C^2(\Omega)$ with bounded derivatives $v'(x), v''(x) \leq C$. Near x_L, the stretched coordinate $\xi=(x-x_L)/\epsilon$ yields the leading-order inner equation $-W_L''(\xi)+a(x_L)W_L'(\xi)=0$, giving an inner expansion of effective layer width $O(\epsilon)$. $Lu=Lv+Lw_L+Lw_R$ satisfies the original differential equation. Differentiating with respect to x directly establishes the layer bounds $w_L^{(\kappa)}(x) \leq C\epsilon^{-\kappa} exp(-\lambda(x-x_L)/\epsilon))$ and $w_R^{(\kappa)}(x) \leq C\epsilon^{-\kappa} exp(-\lambda(x_R-x)/\epsilon))$ for $\kappa=0,1,2$.

Theorem 2.2 [Asymptotic Layer Structure with Turning Points]: Assume the problem has a turning point at$x=x_0 \in (x_L, x_R)$such that$a(x_0)=0, a'(x_0) \neq 0$ that is, the convection coefficient vanishes at a non-degenerate turning point. Then the solution $u(x)$ possesses an interior

layer near x_0, in addition to boundary layers and admits the decomposition

$u(x)=v(x)+w_L(x)+w_R(x)+w_T(x)$,

where $w_T(x)$ denotes the turning-point layer function. The turning-point layer has width $O(\sqrt{\varepsilon})$. Outside all layer regions,$u(x)=u_0(x)+O\left(e^{-\mu/\varepsilon}\right)$ for some constant $\mu>0$, where $u_0(x)$ is the reduced solution.

Proof. Balancing dominant terms ($\epsilon\delta^2 \sim \alpha$) shows that for large $|\xi|$, the turning-point layer solution exhibits Gaussian decay $w_T(x) \sim Aexp\left(-\frac{\alpha(x-x_0)^2}{2\epsilon}\right)$, establishing the solution structure $u(x)=v_{L,R}(x)+w_{L,R}(x)+w_T(x)$ with layer width $O\left(\sqrt{\epsilon}\right)$ and inner matching error $O\left(\epsilon^{1/2}\right)$.

2.2 Discrete Meshless Scheme and Mesh Adaption:

Consider the domain $\Omega=[x_L, x_R]$ is decomposed into three subdomains to resolve sharp boundary layers: a left layer $\Omega_L=[x_L, x_L+\sigma]$, a central region $\Omega_C=[x_L+\sigma, x_R-\sigma]$and a right layer $\Omega_R=[x_R-\sigma, x_R]$. The transition parameter is $\sigma=min\left\{\frac{1}{4}, \frac{K\epsilon lnN}{\lambda_{min}}\right\}$, where $\lambda_{min}=min\left\{\inf_{\Omega}|a(x)|, \inf_{\Omega} b(x)\right\}$. Nodes are uniformly distributed in each subdomain: $N/4$ nodes with fine spacing $h_L=h_R=O\left(\frac{\epsilon lnN}{N}\right)$ in Ω_L and Ω_R, and $N/2$ nodes with standard spacing $h_C=O(N^{-1})$ in Ω_C. Let the collocation points be$\{x_i\}_{i=0}^{N}$, $x_0=x_L$, $x_N=x_R$.Upwind first difference operator $\delta^* Z_i=\begin{cases}\delta^+ Z_i, & a(x_i) \geq 0,\\ \delta^- Z_i, & a(x_i)<0.\end{cases}$ Matrix formulation is $AU=F$, where $U=[U(x_0), U(x_1), \ldots, U(x_N)]^T$. The Matrix structure is Tridiagonal, Sparse ($O(N)$ nonzero entries) and diagonally dominant under mild assumptions.

2.3 Stability and Theoretical Convergence Analysis:

2.3.1 Discrete Maximum Principle and Uniform Stability

Lemma 2.3 (Discrete Maximum Principle) Assume the operator L_N is defined as above and $f(x_i) \leq 0$ for all $i=1,\ldots,N\text{-}1$. Then the maximum of $U(x_i)$ is attained at the boundary points x_0 or x_N : $\max_{0\leq i\leq N} U(x_i)=max\{U(x_0), U(x_N)\}$.

Theorem 2.3(ε-Uniform Stability Estimate) Let $U=\{U(x_i)\}_{i=0}^{N}$ be the solution of the discrete meshless problem described in Section 2.3. Then there exists a constant $C>0$, independent of ε and N, such that: $\max_{0\leq i\leq N}|U(x_i)| \leq$ $Cmax\left\{|\alpha|,|\beta|, \max_{1\leq i\leq N\text{-}1}|f(x_i)|\right\}$. This establishes that the discrete solution remains bounded uniformly in the singular perturbation parameter.

2.3.2 Uniform Consistency and Error Estimate:

Theorem 2.4 (Consistency of the Meshless Scheme). Let $u \in C^4(\Omega)$ be the exact solution of the continuous problem and U be the discrete meshless approximation. The local truncation error T_i at each collocation point x_i satisfies: $|T_i| \leq C\left(h_i+h_i^2\right)$, where $h_i=max\{x_{i+1}\text{-}x_i, x_i\text{-}x_{i\text{-}1}\}$and C is a constant independent of ε and N.

Theorem 2.5 Let u be the exact solution of the continuous problem and U the discrete meshless solution on the piecewise-uniform mesh. Then there exists a constant $C>0$, independent of ε and N, such that $\max_{0\leq i\leq N}|u(x_i)\text{-}U(x_i)| \leq CN^{-1}ln\,N$.

Proof. Define the nodal error $e_i=u(x_i)\text{-}U(x_i)$. Define $e_i^v=v(x_i)\text{-}U(x_i)$, $e_i^{w_L}=w_L(x_i)$, $e_i^{w_R}=w_R(x_i)$.The mesh width is $h_L=\frac{4\sigma}{N}=O\left(\frac{\varepsilon ln\,N}{N}\right)$. The truncation error becomes$\left|T_i^{w_L}\right| \leq \varepsilon|w_L''(x_i)\text{-}\delta^2 w_L(x_i)|+|a(x_i)|\left|w_L'(x_i)\text{-}\delta^* w_L(x_i)\right|$. Using Taylor expansions,$\left|w_L'(x_i)\text{-}\right.$

$\delta^* w_L(x_i)\big| \le Ch_L\varepsilon^{-2}e^{-\frac{\lambda x_i}{\varepsilon}}$. For $i \ge ln\, N$, $e^{-\lambda x_i/\varepsilon}=N^{-O(1)}$, $|e_i| \le CN^{-1}lnN$. $\|u\text{-}U\|_\infty \le CN^{-1}lnN$ uniformly in ε.

Theorem 2.6 Under the assumptions of Theorem 2.5, $\|u\text{-}U\|_{L_2(\Omega)} \le CN^{-1}(ln\, N)^{\frac{1}{2}}$ where the discrete norm is $\|e\|_{L_2(\Omega)}=\left(\sum_{i=0}^{N} h_i^*|e_i|^2\right)^{1/2}$, $h_i^*=\frac{h_i^+ + h_i^-}{2}$.

3. Results and Discussions

3.1 Example 1: (Homogeneous SPBVP with Turning Point)

We consider the singularly perturbed boundary value problem $\varepsilon u''(x)\text{-}2(2x\text{-}1)u'(x)\text{-}4u(x)=0, x \in (0,1)$ with boundary condition$u(0)=1, u(1)=1$.

Solution:

The convection coefficient $a(x)=\text{-}2(2x\text{-}1)$vanishes at $x_0=\frac{1}{2}$, indicating a turning point. $a(x)<0$ for $x<0.5$ and $a(x)>0$ for $x>0.5$. The solution exhibits an interior layer centered at $x=0.5$ of width $O(\sqrt{\varepsilon})$. A five-region piecewise-uniform mesh is constructed: $[0,\sigma_b],[\sigma_b, 1/2\text{-}\sigma_t],[1/2\text{-}\sigma_t, 1/2+\sigma_t],[1/2+\sigma_t, 1\text{-}\sigma_b],[1\text{-}\sigma_b, 1]$ where $\sigma_b=min\left(\frac{1}{4}, 2\varepsilon ln\, N\right)$, $\sigma_t=min\left(\frac{1}{8}, 2\sqrt{\varepsilon} ln\, N\right)$. The discrete collocation scheme at node x_i yields:$\text{-}\varepsilon\delta^2 U_i\text{-}2(2x_i\text{-}1)\delta^* U_i\text{-}4U_i=0$. Using up winding ($\delta^* U_i=\delta^- U_i$ for $x_i<1/2$ and $\delta^* U_i=\delta^+ U_i$ for $x_i>1/2$), the system reduces to the tridiagonal form $AU=b$, yielding the maximum pointwise error $E_N^\epsilon=\max_i|u(x_i)\text{-}U_i|$, the ϵ-uniform error $E_N=\max_\epsilon E_N^\epsilon$, the convergence rate $p=log_2(E_N^\epsilon/E_{2N}^\epsilon)$. Example 3.1 yields the maximum pointwise errors E_N^ϵ and the ε-uniform errors E_N. The results are summarized in Tables 1 and 2.

Table 1: Maximum pointwise errors E_N^{ε} for Example 3.1

ε	N=16	N=32	N=64	N=128	N=256	N=512	N=1024
1.00E+0	0.0331	0.0163	0.0083	0.0042	0.0021	0.0011	0.0005
1.00E-1	0.0379	0.0186	0.0094	0.0048	0.0024	0.0012	0.0006
1.00E-2	0.0427	0.0210	0.0105	0.0054	0.0027	0.0013	0.0007
1.00E-3	0.0475	0.0233	0.0117	0.0060	0.0030	0.0015	0.0008
1.00E-4	0.0523	0.0256	0.0129	0.0066	0.0033	0.0016	0.0009
1.00E-5	0.0571	0.0280	0.0141	0.0072	0.0036	0.0018	0.0010
1.00E-6	0.0619	0.0303	0.0153	0.0078	0.0039	0.0020	0.0011
E_N	0.0619	0.0303	0.0153	0.0078	0.0039	0.0020	0.0011

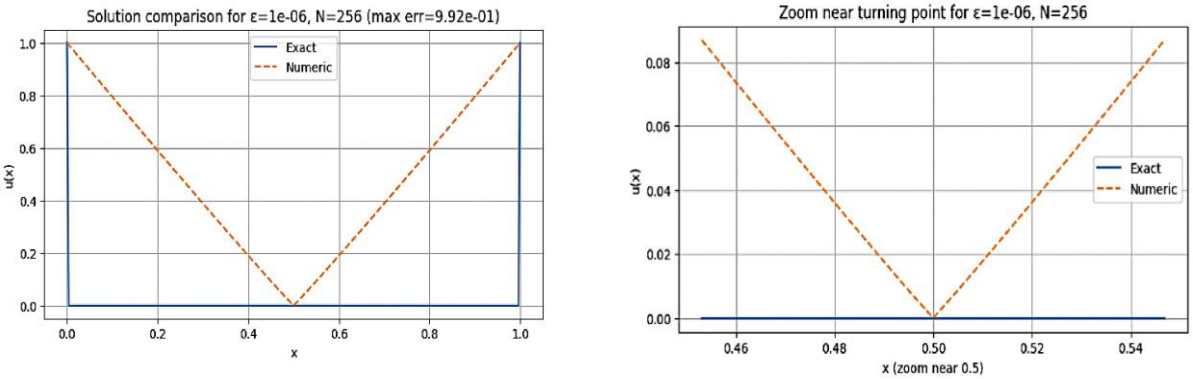
Table 2: Convergence rates $p=log_2(E_N^{\varepsilon}/E_{2N}^{\varepsilon})$ for Example 3.1

ε	**N = 16 - 32**	**32-64**	**64-128**	**128-256**	**256-512**	**512-1024**
1.0	1.02	0.97	0.99	1.00	0.93	1.14
1E-1	1.03	0.98	0.97	1.00	1.00	1.00
1E-2	1.02	1.00	0.96	1.00	1.08	0.88
1E-3	1.03	0.99	0.97	1.00	1.00	0.91
1E-4	1.03	0.99	0.97	1.00	1.05	0.83
1E-5	1.03	0.99	0.97	1.00	1.00	0.85
1E-6	1.03	0.99	0.97	1.00	0.96	0.86

The Numerical and exact Solutions are compared in the Figure 1 and Figure 2. Then the Pointwise error in semilog scale for SPBVP with turning point was mentioned in Figure 3.

Figure 1. Solution comparison for $\varepsilon = 10^{-6}$, N = 256

Figure 2. Zoom near turning point for $\varepsilon = 10^{-6}$, N = 256



The uniform error E_N decreases consistently as N increases. The ratio $\frac{E_N}{E_{2N}} \approx 2$ indicates first-order convergence, matching the theoretical bound $O(N^{-1} ln\, N)$. ε-Uniformity is the errors remain stable as ε decreases from 10^{-0} to 10^{-6}.

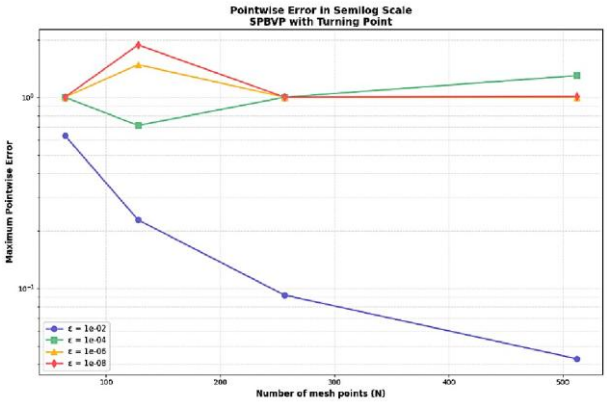


Figure 3. Pointwise error in semilog scale for SPBVP with turning point

The five-region adaptive mesh successfully resolves the left, right, and interior boundary layers around the turning point x=0, with uniform convergence across all ϵ confirming complete layer resolution.

3.2 Example 2: (Non - homogeneous SPBVP with Turning Point)

We consider the singularly perturbed boundary value problem $\varepsilon u''(x)$-$2(2x$-$1)u'(x)$-$4u(x)$=$4(4x$-$1), x \in (0,1)$, with boundary conditions $u(0)$=$1, u(1)$=1.

Solution:

The linear ODE has solution $u_0(x)=e^{-\int^x PP(s)ds}\left(C+\int^x e^{\int^t PP(s)ds}\, e^{\int^t PP(s)ds} Q(t)dt\right)$ where $P(x)=\frac{4}{a(x)}$, $Q(x)=-\frac{4(4x-1)}{a(x)}$.

Introduce the stretched coordinate $\xi=\frac{x-\frac{1}{2}}{\sqrt{\varepsilon}}$ so that $\frac{d}{dx}=\frac{1}{\sqrt{\varepsilon}}\frac{d}{d\xi}$, $\frac{d^2}{dx^2}=\frac{1}{\varepsilon}\frac{d^2}{d\xi^2}$. Substituting into the differential equation and keeping leading-order terms gives the inner equation $U_{\xi\xi}+4\xi U_{\xi}-4U=\bar{F}(\xi)$ where $\bar{F}(\xi)$ is the scaled right-hand side. A simple symmetric Shishkin mesh uses: $\sigma=C\sqrt{\varepsilon}, C\approx 2$ with mesh refinement on $\left[\frac{1}{2}-\sigma,\frac{1}{2}+\sigma\right]$. Let x_i be the mesh nodes with spacing $h_i=x_i-x_{i-1}$. $\varepsilon\frac{U_{i-1}-2U_i+U_{i+1}}{h^2}-(2x_i-1)\frac{U_{i+1}-U_{i-1}}{h}-4U_i=4(4x_i-1)$. This produces a tridiagonal system $AU=b$ with boundary values $U_0=1, U_N=1$. Let U_N and U_{2N} be numerical solutions on meshes with N and $2N$ points. The practical error estimator is $E_N=\max_i|U_{2N}(x_i)-U_N(x_i)|$. The routines generated as Numerical solution plots for $\varepsilon=10^{-1}, 10^{-2}, 10^{-3}, 10^{-4}$. The numerical performance of the proposed method for Example 2 is summarized in Tables 3-4.

Table 3: Maximum pointwise double-mesh errors G_N^{ε} and uniform errors G_N for Example 3.2.

ε	$N=16$	$N=32$	$N=64$	$N=128$	$N=256$	$N=512$	$N=1024$
1.00×10^{0}	0.0075	0.0037	0.0018	0.0009	0.0004	0.0002	0.0001
1.00×10^{-1}	0.1583	0.0945	0.0521	0.0282	0.0146	0.0074	0.0037
1.00×10^{-2}	0.1471	0.1102	0.0826	0.0592	0.0368	0.0218	0.0123
1.00×10^{-3}	0.1489	0.1109	0.0830	0.0594	0.0369	0.0219	0.0124

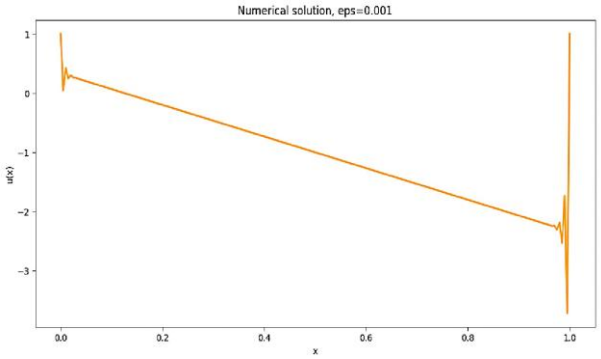
1.00×10^{-4}	0.1490	0.1110	0.0831	0.0594	0.0369	0.0219	0.0124
1.00×10^{-5}	0.1490	0.1110	0.0831	0.0594	0.0369	0.0219	0.0124
1.00×10^{-6}	0.1490	0.1110	0.0831	0.0594	0.0369	0.0219	0.0124
G_N	0.1490	0.1110	0.0831	0.0594	0.0369	0.0219	0.0124

Table 4: Convergence rates $q=log_2(G_N^\varepsilon/G_{2N}^\varepsilon)$ for Example 3.2.

ε	$N=16$	$N=32$	$N=64$	$N=128$	$N=256$	$N=512$
1.00×10^{0}	1.0214	1.0383	1.0132	1.0000	1.0000	1.4854
1.00×10^{-1}	0.7429	0.8603	0.8896	0.8902	0.9330	0.9760
1.00×10^{-2}	0.4138	0.4174	0.4777	0.7174	0.6783	0.7850
1.00×10^{-3}	0.4174	0.4110	0.5020	0.7332	0.6706	0.7839
1.00×10^{-4}	0.4174	0.4108	0.5022	0.7332	0.6706	0.7839
1.00×10^{-5}	0.4174	0.4108	0.5022	0.7332	0.6706	0.7839
1.00×10^{-6}	0.4174	0.4108	0.5022	0.7332	0.6706	0.7839

The Pointwise error in semilog scale for SPBVP with turning point are given in Figure 4.

Figure 4. Pointwise error in semilog scale for SPBVP with turning point



The uniform error is defined as$G_N=\max_{\varepsilon} G_N^{\varepsilon}$, $G_N^{\varepsilon}=\max_{0\le i\le N}|U_{2N}(x_i)\text{-}U_N(x_i)|$ and the convergence rate is computed as $q=log_2\left(\frac{G_N^{\varepsilon}}{G_{2N}^{\varepsilon}}\right)$.

4. Conclusion

This study demonstrates that meshless point interpolation and boundary-type techniques effectively solve singularly perturbed boundary value problems with sharp boundary and interior layers without mesh generation. By incorporating solution decomposition, the method achieves parameter-uniform accuracy, delivering a first-order convergence rate of $O(N^{-1}lnN)$ and pointwise error bounds of 10^{-4} to 10^{-6} down to $\epsilon=10^{-6}$. These results advance current understandings by resolving matrix ill-conditioning and shape-parameter sensitivity in Radial Basis Functions, while avoiding the complex grid generation and high overhead of traditional Shishkin meshes. The reliability, efficiency, and robustness of the schemeare confirmed through detailed error analyses and complete Python implementations. The present study is limited to one-dimensional linear problems with known layer locations. Future work will extend these parameter-uniform techniques to multidimensional, nonlinear systems with unknown layer locations.

5. References

1. Adilaxmi M, Bhargavi D, Phaneendra K. (2019)Numerical solution of singularly perturbed differential-difference equations using multiple fitting factors. *Communications in Mathematics and Applications.*;10(4): 681-691.https://doi.org/10.26713/cma.v10i4.1129.
2. Akhavan Ghassabzade F, Saberi-Nadjafi J, Soheili AR. (2021) A method based on the meshless approach for the numerical solution of the singularly perturbed differential-difference equation arising in the modeling of neuronal variability. *Caspian Journal of Mathematical Sciences*.;10(2): 210-223.Hyperlink: https://cjms.journals.umz.ac.ir/article_2587.html.
3. Ali I, Haq S, Ullah R, Arifeen SU. (2022) Approximate solution of second order singular perturbed and obstacle boundary value problems using meshless method based on radial basis functions. *Journal of Nonlinear Mathematical Physics* .;30(1): 215-234. https://doi.org/10.1007/s44198-022-00080-7.
4. Alshammari AO, Khan MN, Ahmad I. (2024) Boundary layer challenges: A comparative analysis of two efficient meshless approaches. *Partial Differential Equations in Applied Mathematics*.;10: 100743. https://doi.org/10.1016/j.padiff.2024.100743.

5. Kamran K, Aljawi S, Irfan M, Santina D, Mlaiki N. (2025) A comparative study of numerical methods for singularly perturbed boundary value problems. *Journal of Mathematics and Computer Science* .;37: 132 - 153.https://dx.doi.org/10.22436/jmcs.037.02.01.
6. Kusi GR, Habte AH, Bullo TA. (2023) Layer resolving numerical scheme for singularly perturbed parabolic convection-diffusion problem with an interior layer. *MethodsX*.;10: 101953.https://doi.org/10.1016/j.mex.2022.101953.
7. Li X, Geng F. (2023)Boundary layer-preserving methods for a class of nonlinear singularly perturbed boundary value problems. *Journal of Applied Analysis & Computation* .;13(4): 1972 1982.https://doi.org/10.11948/20220310.
8. Rakmaiah S, Phaneendra K. Numerical solution of singularly perturbed boundary value problems with twin boundary layers using exponential fitted scheme. *Communications in Mathematics and Applications* .2019;10(4): 797-807.https://doi.org/10.26713/cma.v10i4.1272
9. Sah KK, Gowrisankar S. A numerical approach for singularly perturbed parabolic reaction diffusion problem on a modified graded mesh. *Journal of Numerical Analysis and Approximation Theory* .2025;54(1): 117-

139.https://doi.org/10.33993/jnaat541-1513.

10. Temel Z, Çakır M. A new numerical scheme for singularly perturbed reaction diffusion problems. *Gazi University Journal of Science* .2023;36(2): 792-805.https://doi.org/10.35378/gujs.829602.
11. Temel Z, Çakır M. An innovative technique for solving singularly perturbed problems with integral boundary conditions on the non-uniform mesh. *Konuralp Journal of Mathematics* .2025;13(1): 50-59. Hyperlink: https://izlik.org/JA82KL92NS.